

# Dalton Transactions

Accepted Manuscript



This is an *Accepted Manuscript*, which has been through the Royal Society of Chemistry peer review process and has been accepted for publication.

*Accepted Manuscripts* are published online shortly after acceptance, before technical editing, formatting and proof reading. Using this free service, authors can make their results available to the community, in citable form, before we publish the edited article. We will replace this *Accepted Manuscript* with the edited and formatted *Advance Article* as soon as it is available.

You can find more information about *Accepted Manuscripts* in the [Information for Authors](#).

Please note that technical editing may introduce minor changes to the text and/or graphics, which may alter content. The journal's standard [Terms & Conditions](#) and the [Ethical guidelines](#) still apply. In no event shall the Royal Society of Chemistry be held responsible for any errors or omissions in this *Accepted Manuscript* or any consequences arising from the use of any information it contains.

Cite this: DOI: 10.1039/c0xx00000x

www.rsc.org/xxxxxx

ARTICLE TYPE

# Phase transfer-based synthesis of HgS nanocrystals†

Lin Han,<sup>ab</sup> Pengfei Hou,<sup>bc</sup> Yan Feng,<sup>b</sup> Hui Liu,<sup>b</sup> Jianling Li,<sup>c</sup> Zhijian Peng<sup>a\*</sup> and Jun Yang<sup>b\*</sup>

Received (in XXX, XXX) Xth XXXXXXXXX 20XX, Accepted Xth XXXXXXXXX 20XX

DOI: 10.1039/b000000x

Phase transfer technique owns a remarkable advantage in the synthesis of inorganic nanomaterials. In comparison with the abundant reports on the preparation of noble metal nanoparticles using phase transfer, the syntheses of semiconductor nanocrystals based on phase transfer technique are still very limited. Herein, we report the systematic studies on the phase transfer-based syntheses of HgS nanocrystals, including the tuning of their morphology/shape by solvents or by temperature. This strategy involves the transfer of Hg(II) ions from aqueous solution to toluene, oleic acid, or oleylamine and the subsequent sulfidation at room or elevated temperature. Further, we extend this phase-transfer based strategy to fabricate the HgS-Au nanocomposites. The studies in this work might present a facile route for producing HgS nanocrystals with desired properties and raise an effective strategy to investigate the influence of morphologies of HgS on the physical/chemical properties of HgS-based various materials.

## 1 Introduction

Phase transfer technique owns a remarkable advantage in the synthesis of inorganic nanomaterials. It allows the synthesis of inorganic nanocrystals of high quality to be performed in organic medium using water-soluble metal salts as starting materials, which are relatively inexpensive and easily obtained.<sup>1,2</sup> Early in 1988, Meguro et al. have reported the transfer of H<sub>2</sub>PtCl<sub>6</sub> into organic solvents from an aqueous solution using dioctadecyldimethylammonium chloride, trioctylmethylammonium chloride, or trioctylphosphine oxide as extractants.<sup>3</sup> The Pt(IV) ions after transfer were reduced by formaldehyde or benzaldehyde in the presence of sodium hydroxide for several hours at 65°C. The Pt nanoparticles obtained in chloroform, cyclohexane, or methylisobutylketone were very stable with diameters of 1.5–2.5 nm. Subsequently in 1989, they extended their transfer method to the preparation of organo gold and alloy Pd/Pt nanoparticles.<sup>4,5</sup>

The often-cited Brust-Schiffrin method is also a phase transfer based approach using water-soluble metal salts to prepare thiol-stabilized nanoparticles.<sup>6,7</sup> In this method, gold metal ions from an aqueous solution are transferred into a hydrocarbon (toluene) phase using tetraoctylammonium bromide as the phase transfer agent. Subsequent reduction takes place in the organic solution using an aqueous NaBH<sub>4</sub> solution in the presence of an alkanethiol, yielding Au particles with average diameter of approximate 2.5 nm.

However, in comparison with the abundant work on preparation of noble metal nanoparticles using phase transfer followed by reduction of the metal precursors,<sup>8–16</sup> the syntheses of semiconductor nanocrystals based on phase transfer technique are still very limited.<sup>17</sup> In this present work, we report our systematic studies on the phase transfer-based syntheses of HgS

nanocrystals, including the tuning of their morphologies by solvents or by temperature. This strategy involves the transfer of Hg(II) ions from aqueous solution to toluene, oleic acid, or oleylamine and the subsequent sulfidation at room or elevated temperature. Further, we extend this phase-transfer based strategy to fabricate the HgS-Au nanocomposites. Considering the great potentials of HgS nanocrystals in optical applications,<sup>18–25</sup> the studies here might present a facile route for producing HgS nanocrystals with desired properties and raise an effective strategy to investigate the influence of morphologies of HgS on the physical/chemical properties of HgS-based various materials.

## 2 Experimental

### 2.1 General materials

Mercury(II) nitrate monohydrate (Hg(NO<sub>3</sub>)<sub>2</sub>·H<sub>2</sub>O, ACS reagent, ≥98.0%), Gold(III) chloride trihydrate (HAuCl<sub>4</sub>·3H<sub>2</sub>O, ACS reagent, ≥49.0% Au basis), dodecylamine (DDA, 98%), element sulfur (S, ≥99.5%), oleylamine (OLA, technical grade, 70%), oleic acid (OA, ≥93%), and tetraoctylammonium bromide (TOAB, 98%) from Sigma-Aldrich, methanol (99%), ethanol (99.5%) and toluene (99.5%) from Beijing Chemical Works, were used as received. All glassware and Teflon-coated magnetic stir bars were cleaned with *aqua regia*, followed by copious rinsing with de-ionized water before drying in an oven.

### 2.2 Phase transfer of Hg(II) ions from aqueous phase to toluene, OLA, or OA

The transfer of Hg(NO<sub>3</sub>)<sub>2</sub> (aqueous solution, 1 mM) from water to toluene followed an ethanol-mediated protocol, which we reported previously.<sup>1</sup> Briefly, 50 mL of 1 mM aqueous Hg(NO<sub>3</sub>)<sub>2</sub> solution was mixed with 50 mL of ethanol containing 1 mL of DDA. After 5 min of stirring, 50 mL of toluene (or OLA, or OA)

was added and stirring continued for another 2 min. Upon the complete transfer of the ions from water, the Hg(II) ion concentration in toluene (or OLA, or OA) was 1 mM. The Hg(II) ions in toluene, OLA, or OA labeled as Hg(II)-T, Hg(II)-OLA, or Hg(II)-OA, respectively, were separated from the aqueous phase and kept for further experiments.

### 2.3 Sulfidation with element sulfur at room or elevated temperature

For the synthesis of HgS at room temperature, 4 mg of elemental sulfur were added to 20 mL of Hg(II)-T in a 50-mL flat-bottom flask. The mixture was stirred for 3 h at room temperature. The solution turned from colorless to brown, indicating the formation of HgS nanoparticles.

While for the sulfidation of Hg(II) ions in OLA or OA, 10 mL of Hg(II)-OLA or Hg(II)-OA was brought to 80°C, followed by addition of 4 mg of element sulfur. The mixture was maintained at 80°C for another 4 h, and allowed to cool down to room temperature. After reaction, the HgS nanocrystals were purified by precipitation with methanol, centrifugation, washing with methanol, and re-dispersed in 10 mL of toluene.

For the morphology tuning of HgS nanocrystals, the Hg(II)-OLA and Hg(II)-OA were mixed first with different volume ratios, and then followed the same protocol for the formation of HgS nanocrystals in OLA or OA. After reaction, the HgS nanocrystals with different morphologies were also purified by precipitation with methanol, centrifugation, washing with methanol, and re-dispersed in toluene.

### 2.4 Synthesis of HgS–Au Nanocomposites

The transfer of Au(III) ions from aqueous solution to toluene was carried out using the Brust-Schiffrin method.<sup>6</sup> Briefly, 50 mL of 1 mM aqueous HAuCl<sub>4</sub> solution was mixed with 50 mL of 1 mM toluene solution of TOAB. After vigorous stirring for 3 min, the phase transfer of Au(III) ions from water to toluene occurred rapidly and completely, as illustrated by the complete bleaching of the color in the aqueous phase. Then for the preparation of HgS–Au nanocomposites, 10 mL of HgS organosol in toluene (prepared from Hg(II)-T) were mixed with 10 mL of Au(III) solution in toluene. The mixture was aged for 12 h to complete the reaction. Additional reducing agent was not required; dodecylamine could reduce Au(III) ions in toluene effectively in the presence of HgS.

### 2.5 Particle characterizations

Fourier-transformed infrared (FTIR) spectra were recorded on a Bruker Alpha-T spectrometer using a KBr pellet technique. The thermogravimetric and differential scanning calorimetry analysis (TG-DSC) was carried out on a Netzsch SAT449F3 Jupiter instrument from the room temperature to 573 K at a heating rate of 5 K/min under the N<sub>2</sub> atmosphere with a flow rate of 20 mL/min. The sample (4 mg) was heated in a standard platinum sample pan. Transmission electron microscopy (TEM) and high resolution TEM (HRTEM) were performed on the JEOL JEM-2100 electron microscope operating at 200 kV with a supplied software for automated electron tomography. For the TEM measurements, a drop of the particle solution was dispensed onto a 3-mm carbon-coated copper grid. Excessive solution was

removed by an absorbent paper, and the sample was dried under vacuum. An energy dispersive X-ray spectroscopy (EDX) analyzer attached to the TEM was used to analyze the chemical compositions of the synthesized nanoparticles. Powder X-ray diffraction (XRD) patterns were recorded on a Rigaku D/Max-3B diffractometer, using Cu K $\alpha$  radiation ( $\lambda = 1.54056 \text{ \AA}$ ). X-ray photoelectron spectroscopy (XPS) was conducted on a VG ESCALAB MKII spectrometer. Samples for XRD and XPS analyses were concentrated from the toluene solution of HgS nanocrystals to 0.5 mL using flowing N<sub>2</sub>. 10 mL of methanol was then added to precipitate the nanoparticles, which were recovered by centrifugation, washed with methanol several times, and then dried at room temperature in vacuum.

## 3 Results and discussion

In the strategy developed in this work, the transfer of Hg(II) ions from water to toluene, OLA, or OA is an important step preceding the synthesis of HgS nanocrystals. It is speculated that a metal complex between Hg(II) ions and DDA was formed in the process, which could be more easily extracted by toluene, OLA, or OA.

### 3.1 Hg(II)-DDA complexes

The formation of Hg(II)-DDA complexes could be verified by the FTIR spectra of the compounds recovered from the organic layer after phase transfer. As shown by Fig. S1a in Electronic Supplementary Information (ESI) for the FTIR spectrum of pure DDA, the bands at 3338 cm<sup>-1</sup>, 2918 cm<sup>-1</sup> and 1473 cm<sup>-1</sup> are attributed to the stretching vibrations of N-H, C-H, and C-N, respectively.<sup>26</sup> In comparison with that of pure DDT, apparent differences could be observed in the N-H and C-N stretching vibrations while other FTIR characteristic peaks were remained in Hg(II)-DDA compounds (ESI Fig. 1b), demonstrating that there was a strong coordination effect between the NH<sub>2</sub> group in DDA and Hg(II) ions. After coordinating with Hg(II) ions, the non-polar tail of DDA enabled the compounds to dissolve easily in a non-polar organic solvent (toluene, oleylamine, or oleic acid).

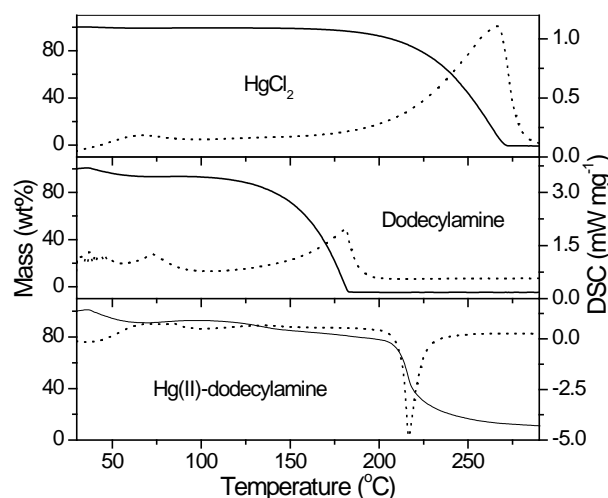


Fig. 1 TG-DSC curves of Hg(NO<sub>3</sub>)<sub>2</sub>, dodecylamine (DDA), and Hg(II)-DDA complexes formed by phase transfer technique.

The complex between Hg(II) ions and DDA was also supported by the TG-DSC analyses. The thermal behaviors of Hg(NO<sub>3</sub>)<sub>2</sub>, DDA, and Hg(II)-DDA complexes examined by TG-DSC in N<sub>2</sub> were demonstrated in Fig. 1. For the DSC curve of Hg(II)-DDA complexes, an abnormal exothermic peak at ca. 217°C was observed. Simultaneously, a sharp weight loss of ca. 65.8%, corresponding to the decomposition of Hg(II)-DDA complexes, began to occur. However, the exothermic peaks could not be found in the DSC curves of both Hg(NO<sub>3</sub>)<sub>2</sub> and DDA, which were featured by the endothermic peaks at ca. 265°C (for Hg(NO<sub>3</sub>)<sub>2</sub>) and at ca. 73°C/180°C (for DDA), respectively.

The ligancy of the complexes formed between Hg(II) ions and DDA could be approximately evaluated by the TG curve of the Hg(II)-DDA compounds recovered from organic phase. If we assume the residue (ca. 11.6%) at the end of heating in nitrogen gas was only pure Hg(NO<sub>3</sub>)<sub>2</sub>, the molar ratio (n) of the DDA and Hg(II) in the Hg(II)-DDA complex can be calculated to be 10, according to the following equation:

$$M_{\text{Hg}(\text{NO}_3)_2} / M_{(\text{DDA})_n} = 11.6/65.8$$

However, as indicated by the TG curve of Hg(NO<sub>3</sub>)<sub>2</sub> (Fig. 1), the decrease in weight of Hg(NO<sub>3</sub>)<sub>2</sub> started to occur at ca. 193°C due to the decomposition of Hg(NO<sub>3</sub>)<sub>2</sub>. Therefore, the actual ligancy of Hg(II)-DDA complexes might be much lower because the weight loss induced by Hg(NO<sub>3</sub>)<sub>2</sub> decomposition cannot be ruled out from the overall weight loss suggested by the TG curve of Hg(II)-DDA.

### 3.2 Synthesis of HgS nanocrystals at room/elevated temperature by sulfidation with element sulfur

The sulfidation of Hg(II) ions in toluene with element sulfur (S) could be conducted at room temperature, which resulted in the formation of mercury sulfide (HgS) nanocrystals. The TEM image showed that the HgS nanocrystals as-prepared in toluene were spherical and monodispersed with an average size of ca. 12.5 nm (Fig. 2a). As illustrated by Fig. S2 in Electronic Supplementary Information (ESI), the EDX analysis produced a Hg/S molar ratio of 57/43, which is in good agreement with the stoichiometric ratio in the final HgS products.

The high-resolution TEM (HRTEM, Fig. 2b) image revealed the lattice planes in these HgS nanocrystals, showing an interplanar spacing of ca. 0.296 nm, which corresponds to the (200) plane of cubic HgS. The successful synthesis of cubic HgS nanocrystals was also confirmed by powder X-ray diffraction (XRD) pattern. As exhibited by ESI Fig. S3, the lines of (111) ( $d = 0.3380$  nm), (200) ( $d = 0.2927$  nm), (220) ( $d = 0.2070$  nm), and (311) ( $d = 0.1765$  nm) diffractions of HgS were clearly identifiable, indicating that the HgS nanocrystals have a cubic lattice structure (JCPDS Card File 890432). The average HgS particle size calculated from the half-width of the (111) diffraction line is ca. 13.2 nm, which agrees well with the TEM result obtained from Fig. 1a.

In addition, the nanocrystals were examined by XPS to confirm their chemical compositions. As shown in ESI Fig. S4, both the Hg 4f region and S 2p region in the final HgS nanocrystals recovered from toluene could be deconvoluted into

one pair of doublet, which was at 100.6 eV and 104.6 eV for Hg, and at 163.5 eV and 168.1 eV for S, respectively, reflecting the ionic state of Hg and S in HgS nanocrystals.<sup>27</sup>

In comparison with the synthesis of HgS nanocrystals in toluene at room temperature, the sulfidation of Hg(II) ions in OLA or OA with element sulfur was performed at elevated temperature. After reaction with element sulfur at 80°C, the as-prepared HgS nanocrystals were precipitated, washed with methanol, and re-dispersed into toluene. For the sulfidation of Hg(II) ions in OLA, as shown by the TEM image (Fig. 2c), the HgS nanocrystals as-prepared were also spherical and had an average diameter of ca. 12.7 nm, close to that prepared in toluene at room temperature. An interplanar spacing of ca. 0.209 nm shown in the HRTEM image of an isolated HgS nanocrystal (Fig. 2d) image suggested a (220) plane of cubic HgS. While for the sulfidation of Hg(II) ions in OA at 80°C, the HgS nanocrystals as-prepared were much bigger and had an average diameter of ca. 56.2 nm, as illustrated by the TEM image (Fig. 2e). Moreover, compared with the HgS nanocrystals prepared by sulfidation in OLA, the morphology and surface of the HgS nanocrystals synthesized in OA at 80°C were very irregular, and therefore it is difficult to differentiate the lattice planes in these HgS nanocrystals, as indicated by the HRTEM image (Fig. 2f).

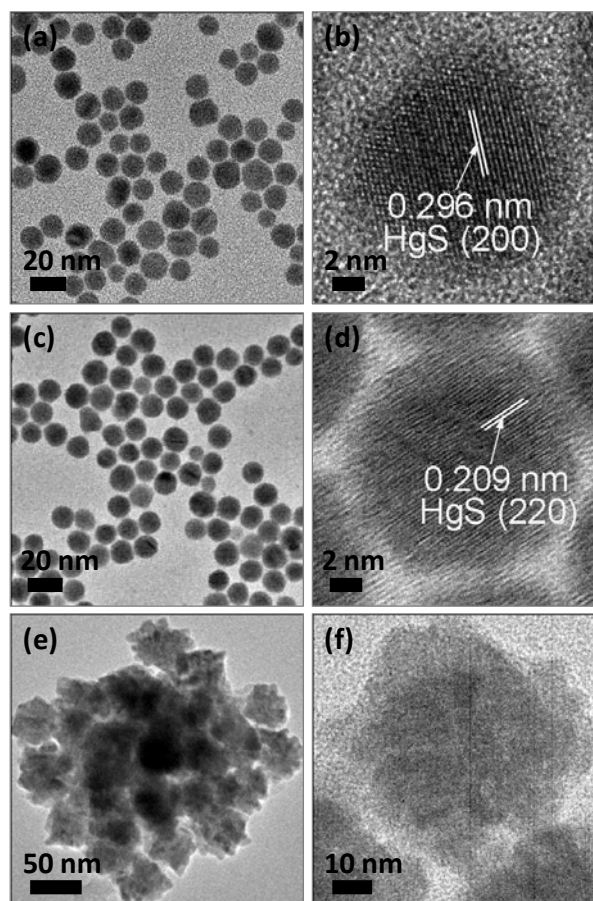


**Fig. 2** TEM images (a,c,e) and HRTEM images (b,d,f) of the HgS nanocrystals synthesized by sulfidation of Hg(II) ions with element sulfur in toluene (a,b) at room temperature, in oleylamine (c,d), and in oleic acid (e,f) at elevated temperature.

In colloidal chemistry method, the nanoparticle could be formed via two processes, i.e. nucleation and crystal growth.<sup>28,29</sup> The nucleation mainly determined by the supersaturation and temperature is the starting point of crystallization, while the particle growth is a process of the assembling of atoms on the surface of nuclei. The growth is controlled by the diffusion of atom to the growing surface followed by the incorporation into the lattice. The incorporation process might be associated with the formation of chemical bond, which could be regarded as the reaction step. Therefore, the particle growth might be regulated by diffusion step and reaction step. Both the diffusion step and the reaction step can be the rate determining step for the particle formation. In this work, the solvents (toluene, OLA, or OA) could affect the diffusion of Hg(II)-DDA as well as its reaction with element sulfur, resulting in the formation of HgS nanocrystals with different size/morphology.

### 3.3 Morphology tuning of HgS nanocrystals by altering OA/OLA volume ratios

As indicated by the TEM images in Fig. 2 (Fig. 2c and 2e), the HgS nanocrystals synthesized in OA and OLA have remarkable difference in size and morphology. This might have implied that the morphology of HgS nanocrystals could be effectively tuned by altering the volume ratio of OA and OLA in the mixture. As we expected, the sulfidation of Hg(II) ions in the mixture of OA/OLA with different volume ratios resulted in HgS nanocrystals with remarkably tuneable morphologies. As shown by the TEM and HRTEM images in Fig. 3, the HgS nanocrystals synthesized in pure OA at 80°C had spherical shape and coarse surfaces (Fig. 3a), while in the mixture of OA and OLA with volume ratios of 1/1, 1/2, and 1/3, HgS nanocrystals with dendritic morphologies were obtained instead, which were featured by the apparently different branches in the HgS nanodendrites (Fig. 3b, c, and d, respectively). When the volume ratio of OA and OLA was decreased to 1/5, HgS nanocrystals

with cubic morphology were the final product, as suggested by Fig. 3e. With the increase of the volume ratio of OA in the OA/OLA mixture, the HgS products were dominated by the nanocrystals with fan-like (Fig. 3f, OA/OLA of 2/3), irregular with a number of triangular (Fig. 3g, OA/OLA of 2/1), and large spherical morphologies (Fig. 3h, OA/OLA of 5/1).

It was noteworthy that varying the volume ratio of OLA and other organic solvent has been a common strategy to synthesize nanomaterials with morphology/shape control. For example, the FePt nanowires/nanorods with tuneable lengths could be obtained by reduction of Pt(acac)<sub>2</sub> and thermal decomposition of Fe(CO)<sub>5</sub> in a mixture of OLA and octadecene with different volume ratios.<sup>30</sup> The shape of the PbS nanocrystals could also be controlled conveniently by varying the volume ratio of solvents in synthesis. Spherical, truncated cubic, and cubic PbS nanocrystals were obtained with OA/OLA volume ratios of 1/9, 1/3, and 3/1, respectively.<sup>1</sup> The mechanism for the morphology tuning of HgS nanocrystals in OA/OLA with different volume ratios was analogous to that for the formation of FePt nanowires with different lengths in OA/OLA mixtures. It is likely that OLA self-organizes into reverse micelles within which the nuclei of HgS are produced. The volume ratio of OLA would definitely affect the morphology of the HgS nanocrystals through affecting the structure of the OLA reverse micelle formed in the mixture. In addition, the slow generation of hydrocarbon amide and water during the condensation reaction between OA and OLA during nanocrystals synthesis,<sup>31,32</sup> would also have influence on the reverse micelles form by OLA in the OA/OLA mixture, and therefore affect the final morphology of the HgS nanocrystals.

As discussed above, the OLA reverse micelle formed in the OA/OLA mixture was essential for the morphology of HgS nanocrystals, which might also be affected by the reaction temperature. After phase transfer, when the sulfidation of Hg(II) ions were carried out in OA/OLA mixture with volume ratio of 1/2 at temperature of 60°C, 100°C, and 150°C, as indicated by the TEM and HRTEM images in Fig. 4, rod-like HgS with a large

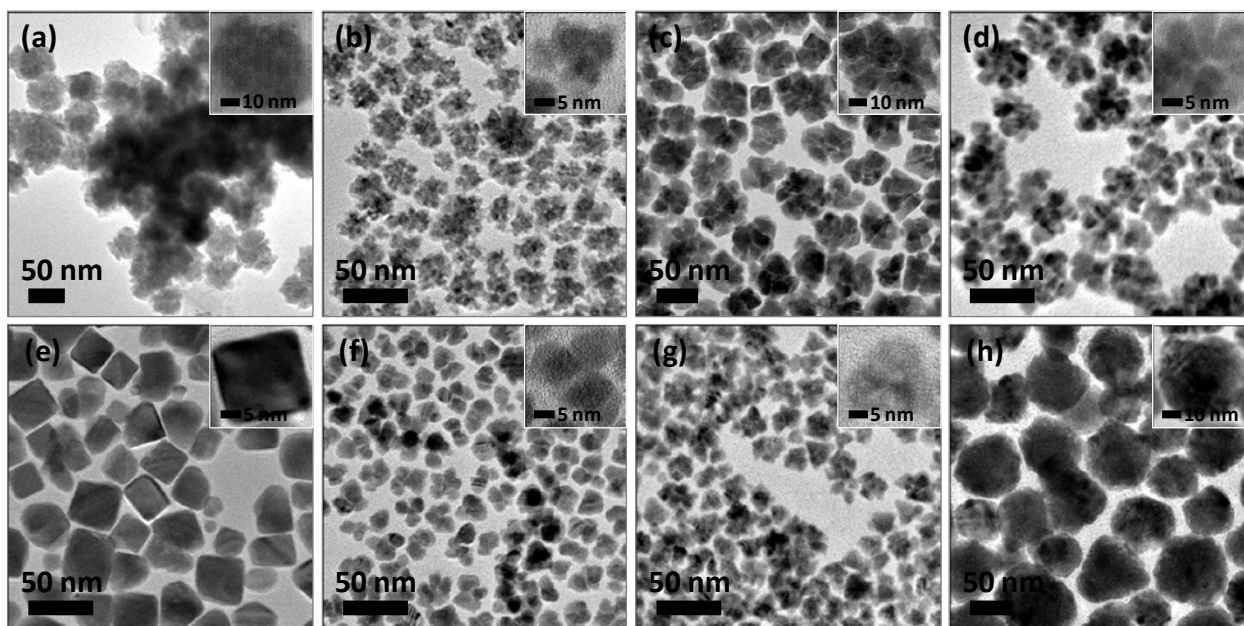


**Fig. 3** TEM images and HRTEM images (insert of each TEM image) of the HgS nanocrystals synthesized at 80°C in OA/OLA with volume ratio of 1/0 (a), 1/1 (b), 1/2 (c), 1/3 (d), 1/5 (e), 2/3 (f), 2/1 (g), and 5/1 (h), respectively.

number of small particles attached, spherical HgS nanocrystals with average diameter of ca. 90.9 nm, and flower-like HgS nanocrystals of ca. 98.3 nm were the majority products, respectively, apparently different from the dendritic HgS nanocrystals prepared at 80°C in same OA/OLA mixture (Fig. 3c). Analogously, since the OLA reverse micelle in OA/OLA mixture are varied at different temperature. The temperature could influence the morphology of the final HgS products through affecting the structure of OLA reverse micelles in the mixture of OA and OLA.

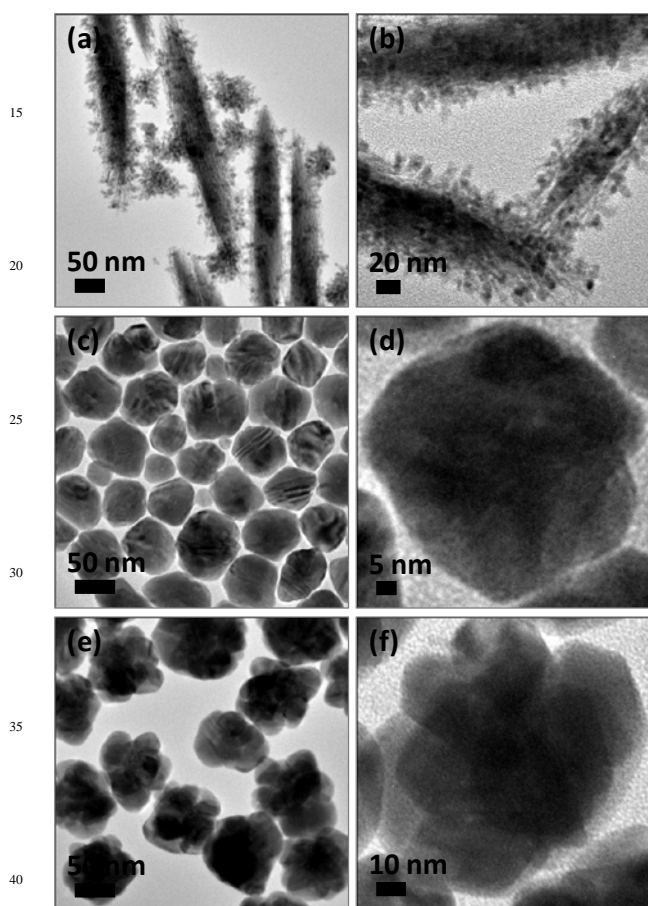


**Fig. 4** TEM images (a,c,e) and HRTEM images (b,d,f) of the HgS nanocrystals synthesized in OA/OLA mixture with volume ratio of 1/2 at 60°C (a,b), 100°C (c,d), and 150°C (e,f), respectively, by sulfidation of Hg(II) ions with element sulfur.

### 3.4 HgS-Au nanocomposites

The increasing interest in nanomaterial synthesis has been devoted towards the development of nanocomposites consisting of semiconductor and noble metals.<sup>33–42</sup> This type of nanostructure combining materials with distinctly different physical and chemical properties is featured by the solid-state interfaces, which oftentimes support the direct charge transfer and lateral strain effect between different components in nanocomposites to yield a unique hybrid nanosystem with multifunctional capabilities and synergistic effects that may not be attainable for the simple sum of the constituents.<sup>43–47</sup>

Upon mixing the HgS nanocrystals formed in toluene and the HAuCl<sub>4</sub> transferred from aqueous phase, we experimentally found that HgS–Au hetero-nanocomposites were the dominant product and their morphology could be significantly affected by the reaction time. No additional reducing agent was needed. Dodecylamine, which was used to transfer the Hg(II) ions from water to toluene, could reduce the Au(III) ions sufficiently in the presence of HgS nanocrystals, analogous to the deposition of Au on Ag<sub>2</sub>S, CdS, and PbS nanocrystals.<sup>1,35,44</sup>

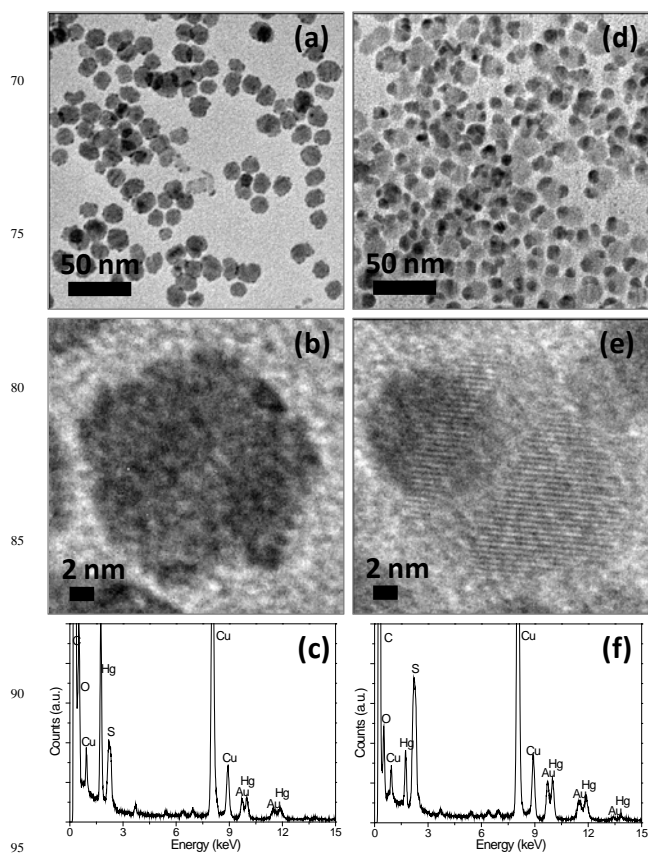


**Fig. 5** TEM images (a,d), HRTEM images (b,e), and EDX analyses (c,f) of the HgS-Au nanocomposites formed by mixing HAuCl<sub>4</sub> and HgS nanocrystals in toluene for 8 h (a,b,c) and 12 h (d,e,f), respectively.

The effect of prolonging the reaction time on the morphologies of the HgS-Au nanocomposites was demonstrated in Fig. 5. The deposition of Au on the surface of HgS nanocrystals in this experiment was carried out in the presence of excess dodecylamine (DDA) and with the HgS/Au molar ratio of 1:1. After mixing the HgS and Au(III) precursors in toluene for 8 h at room temperature, the mixture was turned into light red from pale yellow, indicating the reduction of Au(III) ions. Uniform HgS-Au heterogeneous nanocomposites (Fig. 5a and 5b) were obtained as the dominant product. Isolated Au nanocrystals were not observed. This indicated that Au nucleated preferentially on the existing HgS nanocrystals, instead of homogeneously, under our experimental conditions. Since gold has strong imaging contrast owing to its high electron density,<sup>48</sup> the heterogeneous HgS-Au nanocomposites could be easily identified, although the size of Au domains in the nanocomposites were very tiny. In

most cases, the nucleation and growth of Au occurred at multiple sites on the surface of HgS nanocrystals, similar to the deposition of Au on PbSe<sup>38</sup> or Pt on Ag<sub>2</sub>S nanocrystals.<sup>44</sup> The diameter of the deposited Au domain at this stage was only ca. 1.56 nm. An EDX analysis (Fig. 5c) confirmed that the heterogeneous nanostructures were composed of HgS and Au. The XRD pattern (ESI Fig. S5) of the composite nanomaterials could be indexed as face-centered cubic Au and cubic HgS, corroborating the EDX measurements. The HgS–Au nanocomposites were also studied by XPS (ESI Figs. S6). The doublet at 84.7 and 88.4 eV in Au 4f spectrum could be assigned to metallic Au, while the doublets corresponding to Hg(II) and S<sup>2-</sup> were also clearly identified.<sup>27</sup>

However, when the reaction time was increased to 12 h, the growth of Au on the surface of HgS nanocrystals changed significantly. Instead of deposition at multiple sites, the Au decorated only one-side of the HgS nanocrystals like a dot, forming nanocomposites with dimeric nanostructure (Fig. 5d). The average diameter of PbSe was almost maintained at ca. 12.5 nm, while the size of the Au domain was increased to ca. 7.1 nm. The presence of Au, Hg, and S was also confirmed by EDX analysis of the nanocomposites (Fig. 5f) and the crystalline nature of HgS and Au in the composite nanoparticles was demonstrated by the HRTEM image (Fig. 5e), in which an individual HgS–Au nanocomposite with clear lattice contrast was presented.

The long reaction time induced intriguing reduction of the Au domain numbers on the surface of HgS nanocrystals was analogous to the work reported by Banin and co-workers,<sup>48</sup> in which the two-sided growth of Au tips on CdSe quantum dots or rods was transformed into one-sided growth at relative lower CdSe/Au molar ratio *via* a electrochemical ripening process. Similarly, the experimental phenomena observed in this work could be interpreted by a more common Ostwald ripening process, which is a phenomenon whereby particles larger than a critical size grow at the expense of smaller particles due to their relative stabilization by the surface energy term.<sup>49</sup> After mixing Au(III) ions and HgS in toluene for short time, the Au nucleates and grows at multiple sites on the surface of HgS nanocrystals. With the increase of reaction time, Ostwald ripening occurs when the size of the Au domains reaches a critical size as described in common Ostwald ripening theories. Upon its completion, each composite particle contains one larger gold domain, resulting in the formation of HgS–Au heterodimers.

## 4 Conclusions

In summary, we have developed a phase transfer-based route for the synthesis of HgS nanocrystals, including the tuning of their morphology/shape by solvents or by temperature. This strategy involved the transfer of Hg(II) ions from aqueous solution to toluene, oleic acid, or oleylamine and the subsequent sulfidation at room or elevated temperature. We also extended this phase transfer-based approach to the synthesis of HgS–Au nanocomposites, which were found to be significantly affected by the reaction time. HgS–Au nanocomposites with multiple Au domains of tiny sizes were formed after mixing the Au(III) precursors with HgS nanocrystals in toluene for short time, while HgS–Au heterodimers were obtained instead with the increase of reaction time. The synthetic simplicity may make this work a significant advance in producing semiconductor and

heterogeneously structured nanomaterials for given technological applications.

## Acknowledgement

Financial support from the 100 Talents Program of the Chinese Academy of Sciences, National Natural Science Foundation of China (No.: 21173226, 21376247), and State Key Laboratory of Multiphase Complex Systems, Institute of Process Engineering, Chinese Academy of Sciences (MPCS-2012-A-11, MPCS-2011-D-08, MPCS-2010-C-02) is gratefully acknowledged.

## Notes and references

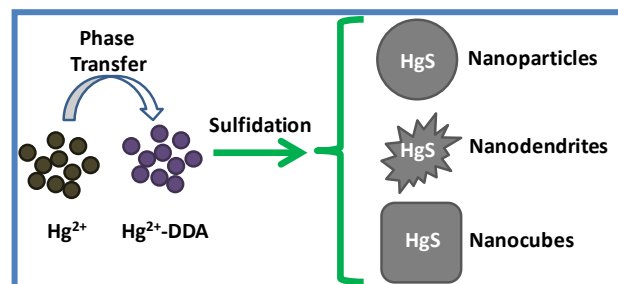
- <sup>a</sup>School of Engineering and Technology, China University of Geosciences, Beijing, China 100083. Fax: 86-10-8232 0255; Tel: 86-10-8232 0255; Email: [pengzhijian@cugb.edu.cn](mailto:pengzhijian@cugb.edu.cn)
- <sup>b</sup>State Key Laboratory of Multiphase Complex Systems, Institute of Process Engineering, Chinese Academy of Sciences, Beijing, China 100190. Fax: 86-10-8254 4814; Tel: 86-10-8254 4915; E-mail: [jiang@mail.ipe.ac.cn](mailto:jiang@mail.ipe.ac.cn)
- <sup>c</sup>State Key Laboratory of Advanced Metallurgy, University of Science and Technology Beijing, 30 College Road, Beijing, China 100083
- †Electronic Supplementary Information (ESI) available: FTIR spectra, EDX analysis, XRD pattern, and XPS spectra for the additional characterization of the nanomaterials synthesized in this study. See DOI: 10.1039/b000000x/
1. J. Yang, E. H. Sargent, S. O. Kelley and J. Y. Ying, *Nat. Mater.*, 2009, **8**, 683.
  2. J. Yang, J. Y. Lee and J. Y. Ying, *Chem. Soc. Rev.*, 2011, **40**, 1672.
  3. K. Meguro, M. Torizuka and K. Esumi, *Bull. Chem. Soc. Jpn.*, 1988, **61**, 341.
  4. K. Meguro, T. Tano, K. Torigoe, H. Nakamura and K. Esumi, *Colloids Surf.*, 1988/1989, **34**, 381.
  5. K. Esumi, M. Shiratori, H. Ishizuka, T. Tano, K. Torigoe and K. Meguro, *Langmuir*, 1991, **7**, 457.
  6. M. Brust, M. Walker, D. Bethell, D. J. Schiffrin and R. Whyman, *J. Chem. Soc., Chem. Commun.*, 1994, 801.
  7. M. Brust, J. Fink, D. Bethell, D. J. Schiffrin and C. Kiely, *J. Chem. Soc., Chem. Commun.*, 1995, 1655.
  8. R. L. Whetten, J. T. Khoury, M. M. Alvarez, S. Murthy, I. Vezmar, Z. L. Wang, P. W. Stephens, C. L. Cleveland, W. D. Luedtke and U. Landman, *Adv. Mater.*, 1996, **8**, 428.
  9. T. G. Schaaff, M. N. Shafiqullin, J. T. Khoury, I. Vezmar, R. L. Whetten, W. G. Cullen, P. N. First, C. Gutierrez-Wing, J. Ascencio and M. J. Jose-Yacamán, *J. Phys. Chem. B*, 1997, **101**, 7885.
  10. M. J. Hostetler, J. E. Wingate, C.-J. Zhong, J. E. Harris, R. W. Vachet, M. R. J. Clark, D. Londono, S. J. Green, J. J. Stokes, G. D. Wignall, G. L. Glish, M. D. Porter, N. D. Evans and R. W. Murray, *Langmuir*, 1998, **14**, 17.
  11. L. A. Porter, Jr., D. Ji, S. L. Westcott, M. Graupe, R. S. Czernuszewicz, N. J. Halas and T. R. Lee, *Langmuir*, 1998, **14**, 7378.
  12. T. G. Schaaff and R. L. Whetten, *J. Phys. Chem. B*, 1999, **103**, 9394.
  13. S. L. Horswell, C. J. Kiely, I. A. O'Neil and D. J. Schiffrin, *J. Am. Chem. Soc.*, 1999, **121**, 5573.
  14. A. C. Templeton, W. P. Wuelfing and R. W. Murray, *Acc. Chem. Res.*, 2000, **33**, 27.
  15. V. L. Jimenez, D. G. Georganopoulou, R. J. White, A. S. Harper, A. J. Mills, D. Lee and R. W. Murray, *Langmuir*, 2004, **20**, 6864.
  16. K. Wikander, C. Petit, K. Holmberg and M.-P. Pileni, *Langmuir*, 2006, **22**, 4863.
  17. H. Shi, X. Fu, X. Zhou and Z. Hu, *J. Mater. Chem.*, 2006, **16**, 2097.
  18. H. D. Riccius and K. J. Siemsen, *J. Chem. Phys.*, 1970, **52**, 4090.
  19. K. A. Higginson, M. Kuno, J. Bonevich, S. B. Qadri, M. Yousuf and H. Mattoussi, *J. Phys. Chem. B*, 2002, **106**, 9982.
  20. P. S. Nair, T. Radhakrishnan, N. Revaprasadu, G. A. Kolawole and P. O'Brien, *J. Mater. Chem.*, 2004, **14**, 581.

21. B. K. Patel, S. Rath, S. N. Sarangi and S. N. Sahu, *Appl. Phys. A*, 2007, **86**, 447.
22. S. K. Mehta, S. Kumar, S. Chaudhary and K. K. Bhasin, *Nanoscale*, 2010, **2**, 145.
23. W. Wichiansee, M. N. Nordin, M. Green and R. J. Curry, *J. Mater. Chem.*, 2011, **21**, 7331.
24. S. Wu, C. Chen, X. Shen, G. Li, L. Gao, A. Chen, J. Hou and X. Liang, *CrystEngComm*, 2013, **15**, 4162.
25. D. Qin, G. Yang, L. Zhang, X. Du and Y. Wang, *Bull. Korean Chem. Soc.*, 2014, **35**, 1077.
26. P. Griffiths and J. A. de Hasseth, *Fourier transform infrared spectrometry* (2<sup>nd</sup> ed.), Wiley-Balckwell, 2007.
27. C. D. Wagner, A. V. Naumkin, A. Kraut-Vass, J. W. Allison, C. J. Powell and J. R. Rumble, *NIST Standard Reference Database 20*, Version 3.2 (Web Version).
28. P. G. Vekilov, *Cryst. Growth Des.*, 2007, **7**, 2796.
29. P. G. Vekilov, *Cryst. Growth Des.*, 2010, **10**, 5007.
30. C. Wang, Y. Hou, J. Kim and S. Sun, *Angew. Chem. Int. Ed.*, 2007, **46**, 6333.
31. M. Chen, T. Pica, Y.-B. Jiang, P. Li, K. Yano, J. P. Liu, A. K. Datye and H. Fan, *J. Am. Chem. Soc.*, 2007, **129**, 6348.
32. H. Wu, Y. Yang and Y. C. Cao, *J. Am. Chem. Soc.*, 2006, **128**, 16522.
33. J. Yang, L. Levina, E. H. Sargent and S. O. Kelley, *J. Mater. Chem.*, 2006, **16**, 4025.
34. S. E. Habas, P. D. Yang and T. Mokari, *J. Am. Chem. Soc.*, 2008, **130**, 3294.
35. J. Yang and J. Y. Ying, *Chem. Commun.*, 2009, 3187.
36. N. Zhao, L. Li, T. Huang and L. Qi, *Nanoscale*, 2010, **2**, 2418.
37. L. Carbone and P. D. Cozzoli, *Nano Today*, 2010, **5**, 449.
38. W. Hu, H. Liu, F. Ye, Y. Ding and J. Y. Yang, *CrystEngComm*, 2012, **14**, 7049.
39. X. Ding, Y. Zou and J. Jiang, *J. Mater. Chem.*, 2012, **22**, 23169.
40. N. E. Motl, J. F. Bondi and R. E. Schaak, *Chem. Mater.*, 2012, **24**, 1552.
41. M. B. Buck, J. F. Bondi and R. E. Schaak, *Nat. Chem.*, 2012, **4**, 37.
42. H. Liu, F. Ye, X. Ma, H. Cao and J. Yang, *CrystEngComm*, 2013, **15**, 7740.
43. R. Costi, A. E. Saunders, E. Elmalem, A. Salant and U. Banin, *Nano Lett.*, 2008, **8**, 637.
44. J. Yang and J. Y. Ying, *Angew. Chem. Int. Ed.*, 2011, **50**, 4637.
45. J. Yang, X. Chen, F. Ye, C. Wang, Y. Zheng and J. Yang, *J. Mater. Chem.*, 2011, **21**, 9088.
46. X. Ding, Y. Zou, F. Ye, J. Yang and J. Jiang, *J. Mater. Chem. A*, 2013, **1**, 11880.
47. H. Liu, F. Ye, H. Cao, G. Ji, J. Y. Lee and J. Yang, *Nanoscale*, 2013, **5**, 6901.
48. T. Mokari, C. G. Sztrum, A. Salant, E. Rabani, U. Banin, *Nat. Mater.*, 2005, **4**, 855.
49. W. F. Ostwald, *Z. Phys. Chem.*, 1897, **22**, 289.

## Phase transfer-based synthesis of HgS nanocrystals

Lin Han,<sup>ab</sup> Pengfei Hou,<sup>bc</sup> Yan Feng,<sup>b</sup> Hui Liu,<sup>b</sup> Jianling Li,<sup>c</sup> Zhijian Peng<sup>a\*</sup> and Jun Yang<sup>b\*</sup>

A phase transfer-based approach was demonstrated for the synthesis of HgS nanocrystals with tuneable morphologies.



Graphical abstract